JAAS

ROYAL SOCIETY OF CHEMISTRY

PAPER

View Article Online
View Journal | View Issue



Cite this: *J. Anal. At. Spectrom.*, 2025, **40**, 421

# Spectroscopic characterization of uranium atoms in uranium-dioxide laser-produced plasma in a high-vacuum environment†

Akira Kuwahara, *[ab] Kenta Murakami,[b] Yuki Mizushima[c] and Hideki Tomita [b]

The expansion dynamics of target particles are crucial for rapid isotope analysis using resonance ionization mass spectrometry (RIMS) combined with laser ablation as an atomization source. The spatial and temporal spectral signatures in laser-produced plasma (LPP) provide insights for applying RIMS to understand the expansion behavior of target particles. In this study, diode laser absorption spectroscopy was employed to observe U atoms in $UO_2$ LPP in a high-vacuum environment ($3.0 \times 10^{-4}$ Pa). Results showed the remarkable differences in the expansion dynamics of U atoms compared to Al atoms. Specifically, the $UO_2$ ablation plume had a double layer due to charged particles, and the spectra of the U atoms do not exhibit clear spectral splitting. Moreover, the U atoms in the $^5L_6$ ground state and low-lying $^5K_5$ meta-stable state (notably, >99% of U atoms generally exist in both energy states) are probed to examine their distributions between the two energy states. The results reveal that approximately 28–38% of the U atoms are distributed in the $^5K_5$ meta-stable state because of thermal excitation. These quantitative insights provide a clear pathway toward advancing the applications of laser ablation.

Received 23rd May 2024
Accepted 3rd December 2024

DOI: 10.1039/d4ja00189c

rsc.li/jaas



## Introduction

Laser ablation (LA) can generate atoms, molecules, ions, electrons, and nanoparticles from a target in the gas phase with intense laser pulses.[1–4] LA has been widely used in laser fabrication, analytical chemistry, and laser deposition.[5–8] As the physics and chemistry of laser-produced plasma (LPP), *i.e.*, its expansion, interaction with an ambient medium, and chemical reactions (dissociation, ionization, and recombination), involve a complex and fast phenomenon, their understanding is challenging for advanced applications.[9–12]

Our previous study was aimed at using LA as an atomization source in resonance ionization mass spectrometry (RIMS).[13] Although achieving a high useful yield (the number of atoms detected per atom consumed) by sputtering from oxide targets with high melting points, particularly $UO_2$, is challenging, LA can enhance the useful yield from $UO_2$.[14–16] However, there are two issues with its application to RIMS.[17–20] First, the nature of atomic behavior in a high-vacuum environment in the range of $10^{-4}$–$10^{-7}$ Pa, which is a pressure range in the RIMS instruments, is unclear. Almost all spectroscopic studies on LPPs have been conducted at moderate-to-atmospheric pressures in the range of $10^2$–$10^5$ Pa.[21–24] However, atomic behavior and spectral signatures are vital for irradiating ionization laser beams to an atomic high-density zone by tuning the timing and position precisely. Second, ejected atoms from a sample surface are thermally excited, and the population of atoms in the ground state decreases in high-temperature environments.[25]

The complex dynamics in LPPs can be understood to access the spectral features of species that have valuable information about plasma parameters, *i.e.*, temperature and density. Although optical emission spectroscopy (OES) provides spatial information easily, OES cannot obtain the kinetic temperature and absolute number density without calibration.[26,27] Tunable Diode Laser Absorption Spectroscopy (TDLAS) with a high wavelength resolution is a powerful tool for directly detecting a specific transition of target atoms.[28–38] As the resonance lines of several metal atoms range from the blue to near-ultraviolet wavelength,[39,40] TDLAS can be utilized.

We have recently addressed the expansion behavior and spectral features of Al atoms in LPP using TDLAS,[12] and spectral splitting behind the plume front and the two-dimensional map for the appearance zone of the splitting are observed. However, the generalizability of these findings to other elements, particularly heavy elements, is unclear. The expansion behavior may cause a difference mainly because of mass difference, and spectral features are strongly affected by it. Therefore, comprehensive spectroscopic investigation is needed for practical use.

[a]*Mechanical Engineering Program, College of Engineering, Shibaura Institute of Technology, Akira Kuwahara 3-7-5 Toyosu, Koto-ku, Tokyo 135-8548, Japan. E-mail: akuwa@sic.shibaura-it.ac.jp; Tel: +81 3 5859 8060*

[b]*Department of Applied Energy, Graduate School of Engineering, Nagoya University, Aichi 464-8603, Japan*

[c]*Department of Mechanical Engineering, Graduate School of Integrated Science and Technology, Shizuoka University, Shizuoka 432-8561, Japan*

† Electronic supplementary information (ESI) available. See DOI: https://doi.org/10.1039/d4ja00189c

This study describes the expansion behavior and spectral features of U atoms generated by the LA of $UO_2$ using TDLAS. In particular, the differences between Al and U atoms are discussed.[12] Moreover, the population distribution of U atoms in both the $^5L_6$ ground state and $^5K_5$ meta-stable state is discussed. This discussion has two important intentions related to RIMS. First, the U atoms in both states account for over 99%, and thus, the behavior of almost every U atom can be tracked.[41] Second, the generation of meta-stable atoms decreases the number of atoms in the $^5L_6$ ground state. The population distribution is compared with those generated by ion beams,[25] and the applicability of LA for RIMS is mentioned.

## Experimental

Our experimental apparatus comprised the LA and TDLAS systems. A conceptual diagram is shown in Fig. 1.[12] The second harmonic radiation from an Nd:YAG laser (GCR-190-10, Spectra-Physics, 532 nm, 17 ns) was used for LA. The pulse energy and repetition rate were 20 mJ and 10 Hz, respectively. The focused spot size was ~120 μm (full width at half maximum) at the sample surface, which was generated using a plane-convex lens (LA1708-YAG, Thorlabs) and measured using a beam profiler (LBP2-VIS, Newport).

A cubic vacuum chamber was evacuated using a pumping system, which comprised a scroll pump (SDM-320-TVL2, ANEST IWATA) and a turbo molecular pump (TG220FVAB, Osaka Vacuum). A target pellet (diameter of 8.7 mm and height of 2.4 mm) with ~76% $UO_2$ (depleted U) was used as a surrogate for nuclear fuel and mounted in the chamber. The pellet was a sintered pellet mainly containing $UO_2$, $CeO_2$, $Nd_2O_3$, and $MoO_3$ at the weight percentages of 75.7%, 13.1%, 3.8%, and 2.0%, respectively. LA experiments were conducted at the background pressure of $3.0 \times 10^{-4}$ Pa, and the pressure was monitored using a crystal/cold cathode combination gauge (CC-10, Tokyo Electron).

For the TDLAS measurements, external cavity diode lasers (DL pro and DL 100, Toptica Photonics) were used as probe lasers. The diameter of the collimated probe beam was ~1.0 mm. Accurate absorption profiles were obtained by scanning the wavelength of the probe laser beams with a repetition frequency of 0.98 Hz, and the scanning widths of the DL pro and DL 100 were approximately 40 and 20 GHz, respectively. As the time scale of LPP evolution ($10^{-8}$ s) was considerably faster than the scanning of the probe laser ($10^0$ s), an absorption signal at one wavelength per shot was acquired and signals from 100 shots were accumulated to reconstruct an absorption profile. Their wavelengths were monitored using a wavemeter (WA6-600, HighFinesse GmbH). The transmitted laser beam was detected using an avalanche photodiode (APD430A2/M, Thorlabs). An optical band-pass filter (FB390-10, Thorlabs) and a notch filter (NF533-17, Thorlabs) were attached in front of the detector. Signals were recorded using an oscilloscope with 12 bit vertical resolution (DL850, Yokogawa) at a maximum sampling rate of 100 MS $s^{-1}$. The relative positions along the *Z*-axis direction between the $UO_2$ pellet and the height of the probe laser beam were changed in two single-axis translation stages (PT1/M, Thorlabs).

## Results and discussion

Two electron transitions of U atoms from the $^5L_6$ ground state and the $^5K_5$ meta-stable state were selected as absorption lines, whose wavelengths were 394.3816 (0–3.15 eV) and 404.2750 nm (0.08–3.15 eV) in air, respectively. The details of the two transitions are presented in Table 1. Both transitions had high gf

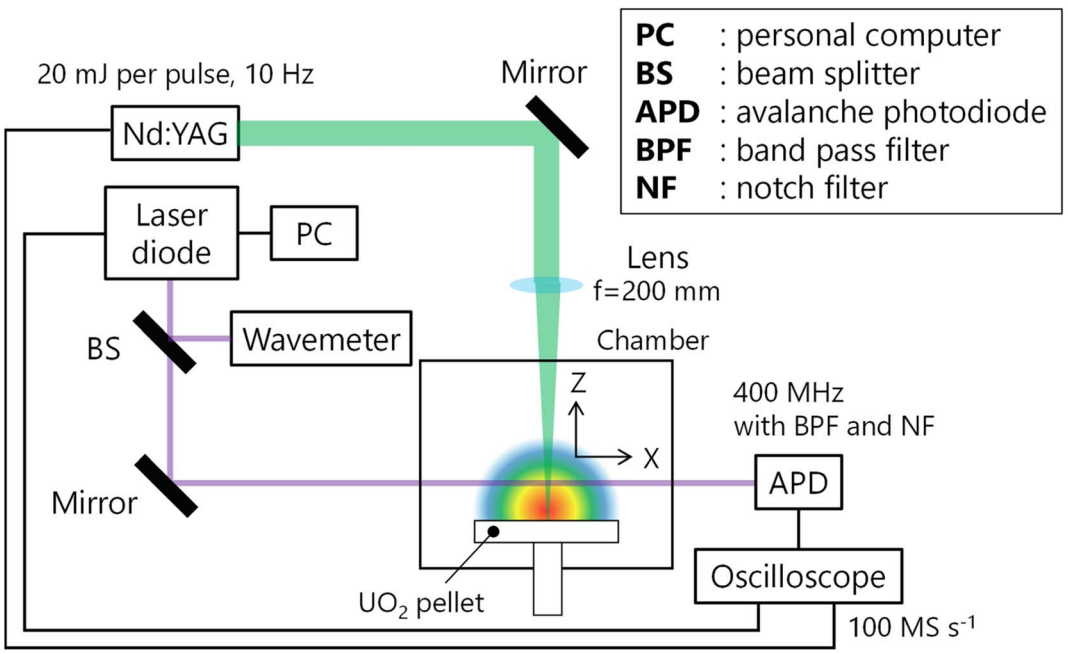


Fig. 1 Conceptual diagram of laser ablation and tunable diode laser absorption spectroscopy.

 

Table 1 Details of the absorption lines[42]

| Parameters | Ground state | Meta-stable state |
|---|---|---|
| Wavelength in air | 394.3816 nm | 404.2750 nm |
| Log(gf) | 0.099 | 0.052 |
| $A$ | $4.141 \times 10^7$ s$^{-1}$ | $3.537 \times 10^7$ s$^{-1}$ |
| $J$ | 6–6 | 5–6 |

values and facilitate a highly sensitive detection of U atoms. Two types of absorption measurements were performed: fixed mode and wavelength scanning mode. The former was used for optical time-of-flight (ToF) measurements to evaluate the propagation velocity of the plume front. The latter was performed to obtain absorption profiles by accumulating fast signals, as described in the Experimental section.

### Temporal profiles of the absorbance of two absorption lines

The temporal profiles of transmittance signals ($I/I_0$) are shown in Fig. 2. The absorbance $A(\nu)$ was calculated by the Lambert–Beer law as,

$$A(\nu) = a(\nu)l = -\ln\left(\frac{I}{I_0}\right) \quad (1)$$

where $a(\nu)$ is the absorption coefficient, $\nu$ is the frequency, and $l$ is the optical pass length. These profiles were observed using the optical ToF measurements in the fixed wavelength mode with the center frequency of the absorption line from the $^5L_6$ ground state. The time on the horizontal axis represents the delay time from the pulsed laser irradiation. The transistor-to-transistor logic signal from the Q-switch laser was used as a trigger signal, and the time jitters of the synchronization signal and pulse timing of the Nd:YAG laser were ≤1 and <0.5 ns, respectively.

The background signal fluctuations were derived from the intensity fluctuations of the probe laser beam and shot-by-shot U density variations. The limit of detection (LOD) for the absorbance in the TDLAS measurements was approximately $1.7 \times 10^{-2}$. Considering the abundance of $^{235}$U in the depleted U (<0.72%), an absorption signal of $^{235}$U cannot be detected. The LOD for $^{235}$U was also previously mentioned.[43]

The absorption signals of U atoms in the $^5L_6$ ground state were observed at a height of 10 mm away. The arrival time of the temporal profiles for U atoms at 1 mm was approximately 660 ns, and their absorbance reached over 1.7. Inside the plume front, optically thick plasma was formed, which is defined when the optical thickness, expressed as al, exceeds 1. The temporal profiles at all vertical positions had absorbance peaks, and the peak values decreased with the vertical position. This is due to complicated factors, which include the propagation of the plume front and the extension of the contact layer into the $Z$-axis direction.[44,45] These factors caused the decrease in the local concentration of U atoms. Another route for the decrease in the absorbance peak might involve the recombination of U atoms as described below.

At the heights of 1, 3, and 5 mm, the temporal profiles had a single peak because of the single-component distribution of atomic velocities. Contrarily, at the height of 10 mm, two peaks appeared as shown in the inset figure, attributed to the double-layer effect or plume splitting.[46–50] This splitting was induced by the spatial charge separation inside the plume core and U atoms were divided into two atomic groups: fast and slow components. The fast atomic group was affected by ions accelerated by an electric field. Notably, slight distortions in the profiles at 3 and 5 mm were visible before the peaks appeared. Thus, two atomic groups were already present at the early stage, and those differences in the absorption signals became evident.

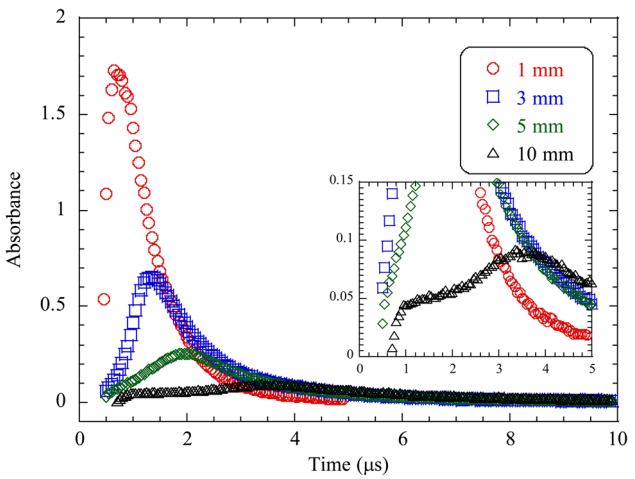


Fig. 2 Temporal profiles of the absorbance at typical vertical positions. The enlarged inset shows a partially enlarged figure. The temporal profile at 10 mm has a double-layer configuration.

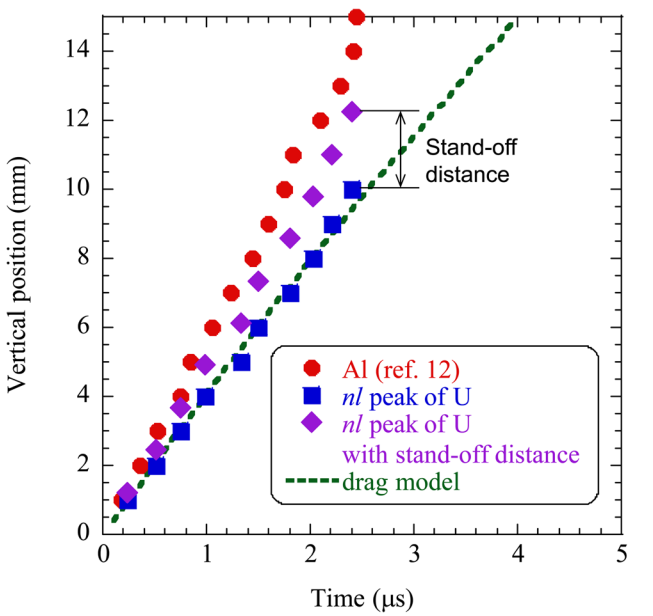


Fig. 3 Position–time plots of the U and Al atoms. Plots show the arrival time of each absorbance peak. The simple hemispheric model was considered to determine the range of the densest point of U atoms and the purple diamond makers indicate the top position of the plume.

### Expansion velocity of the laser-produced plasma front in the *z*-axis direction

Position–time plots are shown in Fig. 3. These plots show the arrival times of the absorbance peaks at each vertical position, where the peak position of the absorbance coincides with the peak position of the column density *nl* as described below. Here, the plume front on the time axis is defined as the densest point inside the plume. The evaluation of the densest point through the column density *nl* by DLAS requires consideration of the decrease of the number density *n* and the extension of the optical pass length *l*. A simple geometrical model of the plume with a hemispherical plume as described in the ESI† can estimate the top position of the plume and the distance between the top position and *nl* peak in the model is defined as the stand-off distance. For instance, the stand-off distance at the height of 10 mm was calculated to be 2.3 mm and the densest point was estimated to lie within the range of 10–12.3 mm. In Fig. 3, the top positions considering the stand-off distance are indicated by purple diamond markers, and the densest points are within the stand-off distance.

First, the propagation velocity of the plume front was evaluated to be approximately $3.0 \times 10^3$ m $s^{-1}$ by the ToF measurement at an interval of 1 mm. The velocity of the U atoms was slower than that of the Al atoms, $5.4 \times 10^3$ m $s^{-1}$.[12] The LPP expansion in a high-vacuum environment can be described using the drag model, $R = R_0\{1-\exp(-\beta t)\}$, where $R_0$ is the stopping distance of the plume, and $\beta$ is the slowing coefficient.[51–57] Fitting results showed that $R_0 = 64.2$ and $\beta = 6.6 \times 10^4$ $s^{-1}$. The experimental plots corresponded to the drag model. The results suggested that the U atoms remained close to the surface of the target.

### Spectral signatures of uranium atoms in the $^5L_6$ ground and $^5K_5$ excited states

The typical spectra of U atoms in the ground and excited states are shown in Fig. 4. All spectra at the heights of 1, 3, 5, and 10 mm are shown in the ESI.† The spectral signatures varied with the time and position. Two types of signatures were observed: one with a single peak and the other with double peaks, attributed to Doppler splitting.[44] The spectra of the Al atoms behind the plume front showed double peaks, whereas almost all those of the U atoms had a single peak during the plume propagation. Only the spectra of the U atoms before the plume front showed slight features of the Doppler splitting, as shown in Fig. 4(a-1), (b-1), and (b-2). However, its appearance zone on the temporal and spatial axis of the U atoms was

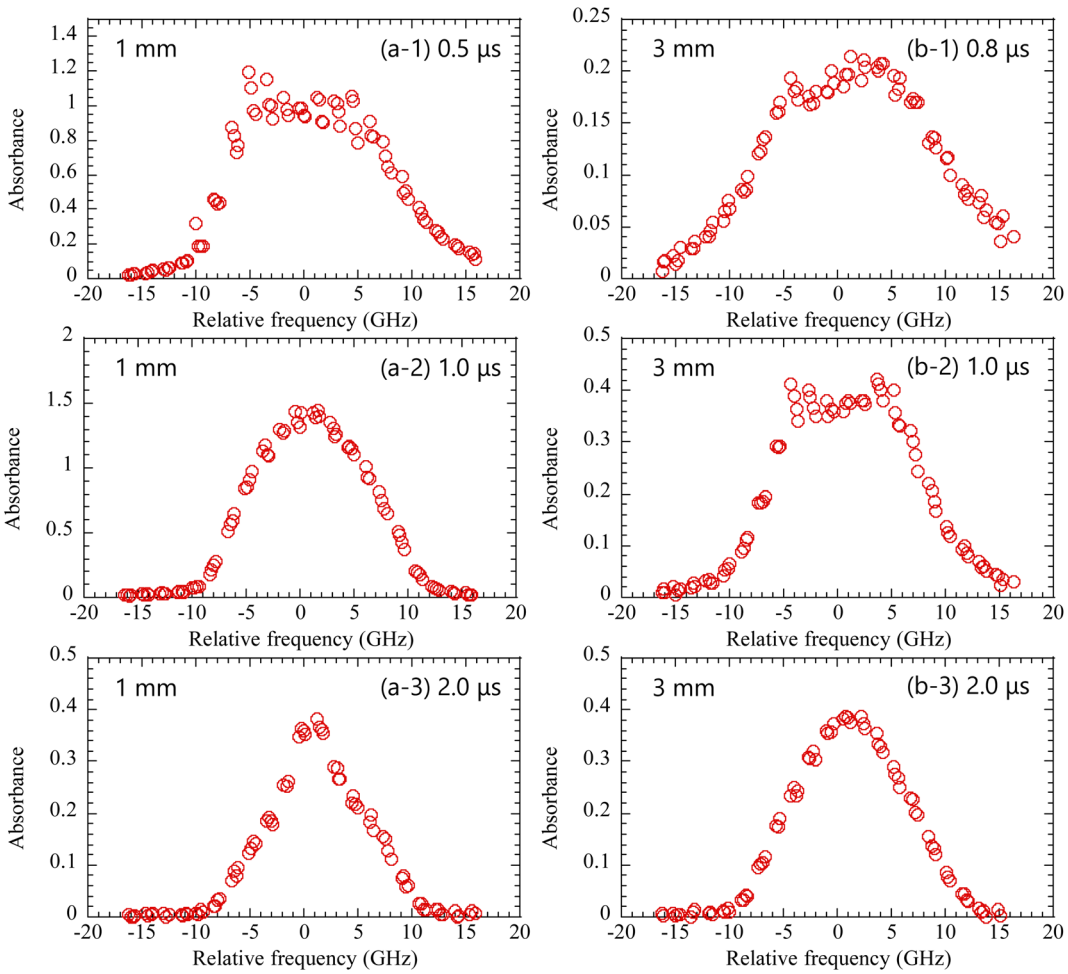


Fig. 4 Absorption spectra of U atoms in the $^5L_6$ ground state at the height of (a-1)–(a-3) 1 mm and (b-1)–(b-3) 3 mm.

 

completely different from that of the Al atoms.[12] In these spectra as shown in Fig. 4, the Doppler splitting occurred before the peaks were observed. Notably, the Doppler splitting stemmed from the lateral motions of the atoms and the formation of a quasi-cavity. This is closely related to the aforementioned plume splitting and suggests that slight features appeared between the fast and slow components of the U atoms. Thus, for $UO_2$, a quasi-cavity was not formed because of the existence of the slow components. Additionally, as the slow one stayed closer to the sample surface compared with the fast one, the Doppler splitting did not occur, even behind the plume front position of the slow component.

As the spectra after passing through the plume front of the fast one contained both vertical and lateral components, the kinetic temperature could not be correctly estimated from the Doppler broadening. Its broadening corresponds to the order of $10^5$ K, which is one order of magnitude greater than those of the Al atoms.[12] At the early stage, the influence of the Lorentz broadening is not negligible because of the relatively high density of electrons.[23]

### Column densities of the uranium atoms in the $^5L_6$ ground and $^5K_5$ excited states

The column density ($nl$) can be calculated from the frequency-integrated value of the absorbance as follows

$$nl = \left(\frac{e^2}{4\varepsilon_0 m_e c}\cdot f_{ij}\right)^{-1}\cdot\int a(\nu)\mathrm{d}\nu \qquad (2)$$

where $e$ is the elementary charge, $\varepsilon_0$ is the permittivity of vacuum, $m_e$ is the mass of an electron, $c$ is the speed of light, and $f_{ij}$ is the oscillator strength of an absorption transition. The temporal profiles of the column density at the height of 3, 5, and 10 mm are shown in Fig. 5. The profile at the height of 1 mm is shown in the ESI (Fig. S3)† since the diameter of the probe beam and the plume size are comparable at the early stage and the inside of the plume cannot be spatially resolved enough. The peak value of the column density in the $^5L_6$ ground state at 3 mm was approximately $3.5 \times 10^{12}$ cm$^{-2}$ and was lower than that of the Al atoms in the ground state, which was $1.3 \times 10^{13}$ cm$^{-2}$.[12]

The column density in the $^5L_6$ ground state drastically decreased in the vertical direction, specifically from 1 mm to 32% at 3 mm and 13% at 5 mm. In contrast to $Al_2O_3$, over 70% of the Al atoms in the ground state remained at the height of 5 mm, as shown in the ESI (Fig. S2).† A possible explanation for these results might be that the lifetime of atoms includes various chemical reactions.[58–65] Finko *et al.* (2018) showed the numerical simulation of U-LPP dynamics in atmospheric pressure.[58,59] This theoretical study reported that the main loss pathway of U atoms in the plume core is a U + O associative ionization channel. Kautz *et al.* (2020) conducted spectroscopic investigations using emissions from U atoms and UO molecules.[60] This experimental study revealed that U atoms and UO molecules co-exist within the plume, and the recombination can be correlated with the plasma temperature. However, the conventional TDLAS is a path-integrated measurement over the optical path length, which is an important limitation.[37] As mentioned above, the kinetic temperature obtained from TDLAS is not applicable for spatially resolved chemical reactions.

### Population distribution in the $^5L_6$ ground and $^5K_5$ excited states

The column density ratios of the U atoms in the $^5L_6$ ground state to the $^5K_5$ excited state at three vertical positions are shown in Fig. 6. All ratios indicate the same temporal variations, and they

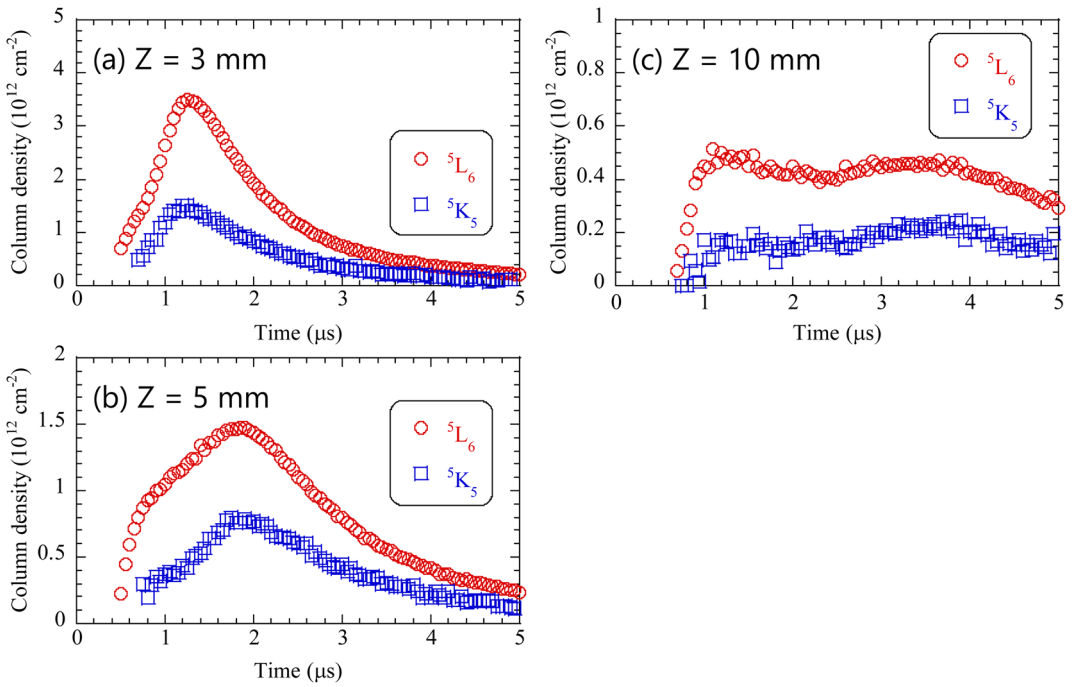


Fig. 5 Column densities of the U atoms in the $^5L_6$ ground state and the $^5K_5$ meta-stable state at the heights of (a) 3, (b) 5, and (c) 10 mm.

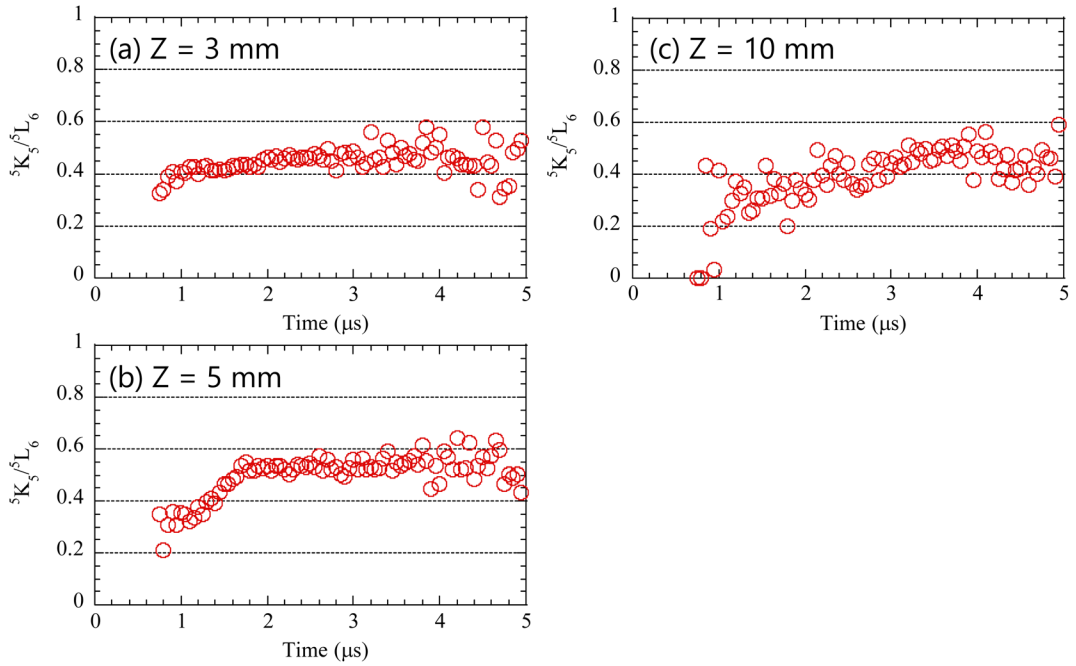


Fig. 6 Column density ratios of the U atoms in the $^5L_6$ ground state and the $^5K_5$ meta-stable state at the heights of (a) 3, (b) 5, and (c) 10 mm.

have two regions: one is the transient region, and the other is the stationary region. At the early stage, the ratios increased with time. In contrast, after the plume front passed, the ratios moved to the stationary regions. In this region, the ratios ranged from 0.4 to 0.6, and the corresponding occupancy of atoms in the $^5L_6$ ground state was 28–38%.

Phillips *et al.* (2023) conducted an experimental study on the thermodynamic equilibrium of the U-LPP at a pressure of 40 Torr.[66] This study suggested that the excitation temperature decreases and reaches the local thermodynamic equilibrium (LTE) at the later stage (<100 μs). These studies dealt with metallic U samples, and the ambient pressure is moderate ambient pressure. Nevertheless, the knowledge could be applied to the U-LPP in a high-vacuum environment as a common explanation,[67] since the pressure inside the contact layer was high enough (>$10^5$ Pa).[68] Thus, the stationary region, as shown in Fig. 6, indicates the LTE condition in the slow component.

Savina *et al.* (2018) investigated the relative population ratio of the U atoms in the $^5L_6$ ground state to the $^5K_5$ excited state generated by ion bombardment with 3 keV $Ar^+$.[25] This population ratio ranged from approximately 0.5 to 0.6. The atomization from $UO_2$ by LA had relatively high occupancy in the $^5L_6$ ground state. The time zone being irradiated by the ionization laser would be limited to the timing during the propagation of the plume front, and the occupancy level would increase. A note of caution is due here that the column density of the U atoms decreases close to the sample surface, and the spatial zone becomes narrower than that of the Al atoms.

## Conclusion

This study aimed to examine the expansion dynamics and spectral features of U atoms to apply $UO_2$ LPP to RIMS. The spatial and temporal spectra of the U atoms were obtained by probing U atoms in the $^5L_6$ ground state and $^5K_5$ meta-stable state generated from the $UO_2$ pellet. The evidence from this study suggests that, in general, the absorption spectra of U atoms have different features compared with those of Al atoms. In particular, the findings highlight that U atoms were separated into two components by plume splitting, and the absorption spectra of the U atoms did not have the clear Doppler splitting feature. However, a glimpse of Doppler splitting was observed before the plume front. Thus, these signatures supported that U atoms moving in the lateral direction were detected between the arrival times of the fast and slow components of U atoms.

The column densities in the $^5L_6$ ground state and $^5K_5$ meta-stable state were evaluated using the integrated line profiles, and the peak reached approximately $3.5 \times 10^{12}$ $cm^{-2}$ at the height of 3 mm. The column density of the U atoms decreased closer to the sample surface than those of Al atoms. The population distribution of the two energy states showed a transition to LTE in the plasma plume at the later stage, which ranged from 28% to 38%. Thermal excitation by LA made fewer U atoms in the $^5K_5$ meta-stable state than by the bombardment of ion beams.

The study contributes to our understanding of the spectral features and expansion dynamics for heavy elements in a high-vacuum environment. For the application of LA to RIMS, the findings illustrate how available U atoms for resonance ionization are spatially and temporally narrower than in the case of Al atoms. However, the current investigation did not include the consideration of chemical processes, particularly oxidation. Further studies should evaluate the kinetic temperature with spatial point-by-point measurements and probe atomic and molecular oxygen.

## Data availability

The data supporting this article have been included as part of the ESI.†

## Author contributions

Conceptualisation and writing—original draft: A. K.; funding acquisition: A. K.; investigation: A. K., K. M.; writing—review and editing: A. K., K. M., Y. M., H. T.

## Conflicts of interest

There are no conflicts to declare.

## Acknowledgements

This work was partially supported by JSPS KAKENHI Grant Numbers JP21H01858 and 24K01401, and the ISIJ Research Promotion Grant. We are truly grateful to T. Shimoyama, Prof. Y. Tsuji, and Prof. S. Yoshihashi for providing technical support.

## References

1 B. N. Chichkov, C. Momma, S. Nolte, F. von Alvensleben and A. Tunnermann, *Appl. Phys. A*, 1996, **63**, 109.
2 E. G. Gamaly, A. V. Rode, B. Luther-Davies and V. T. Tikhonchuk, *Phys. Plasmas*, 2002, **9**, 949.
3 A. Balachandran, S. P. Sreenilayam, K. Madanan, S. Thomas and D. Brabazon, *Results Eng.*, 2022, **16**, 100646.
4 A. Kuwahara, Y. Mizushima, M. Matsui, T. Kozuka and N. Mase, *RSC Adv.*, 2022, **12**, 9304.
5 C. Phipps, *Laser Ablation and its Applications*, Springer, 2007.
6 I. Strashnov, I. Izosimov, J. D. Gilmour, M. A. Denecke, J. Almiral, A. Cannavan, G. Chen, C. Dissanayake, I. Doroshenko, T. Elghali, E. Enston, B. R. Fernando, G. Kasozi, S. Kelly, M. Maqsood, S. A. Muhammad, C. Muryn, A. L. Pomerantsev, D. K. Singh, G. Smith, F. Taous, C. Webb, D. Williamson, Z. Xu, S. Yang and A. Zitek, *J. Anal. At. Spectrom.*, 2019, **34**, 1630.
7 K. B. Masood, P. Kumar, M. A. Malik and J. Singh, *Emergent Mater.*, 2021, **4**, 737.
8 S. S. Harilal, B. E. Brumfield, N. L. LaHaye, K. C. Hartig and M. C. Phillips, *Appl. Phys. Rev.*, 2018, **5**, 021301.
9 S. S. Harilal, M. C. Phillips, D. H. Froula, K. K. Anoop, R. C. Issac and F. N. Beg, *Rev. Mod. Phys.*, 2024, **96**, 019901.
10 T. A. Labutin, V. N. Lednev, A. A. Ilyin, A. M. Popov and J. Anal, *At. Spectrosc.*, 2016, **31**, 90.
11 E. J. Kautz, J. Yeak, B. E. Bernacki, M. C. Phillips and S. S. Harilal, *J. Anal. At. Spectrom.*, 2020, **35**, 1574.
12 A. Kuwahara, K. Murakami, H. Tomita, K. Sawada and Y. Enokida, *J. Anal. At. Spectrom.*, 2022, **37**, 2033.
13 D. E. Goeringer, W. H. Christie and R. E. Valiga, *Anal. Chem.*, 1988, **60**, 345.
14 M. R. Savina, B. H. Isselhardt, A. Kucher, R. Trappitsch, B. V. King, D. Ruddle, R. Gopal and I. Hutcheon, *Anal. Chem.*, 2017, **89**, 6224.
15 M. R. Savina, R. Trappitsch, A. Kucher and B. H. Isselhardt, *Anal. Chem.*, 2018, **90**, 10551.
16 S. L. Ziegler and B. A. Bushaw, *Anal. Chem.*, 2008, **80**, 6029.
17 T. Sakamoto, M. Morita, K. Kanenari, H. Tomita, V. Sonnenschein, K. Saito, M. Ohashi, K. Kato, T. Iguchi, T. Kawai, T. Okumura, Y. Satou and I. Wakaida, *Anal. Sci.*, 2018, **34**, 1265.
18 R. E. Russo, X. Mao, J. J. Gonzalez, V. Zprba and J. Yoo, *Anal. Chem.*, 2013, **85**, 6162.
19 D. Schönenbach, F. Berg, M. Breckheimer, D. Hagenlocher, P. Schönberg, R. Haas, S. Amayri and T. Reich, *Anal. Bioanal. Chem.*, 2021, **413**, 3987.
20 D. Willingham, M. R. Savina, K. B. Knight, M. J. Pellin and I. D. Hutcheon, *J. Radioanal. Nucl. Chem.*, 2013, **296**, 407.
21 M. Miyabe, M. Oba, H. Iimura, K. Akaoka, Y. Maruyama and I. Wakaida, *Appl. Phys. A*, 2010, **101**, 65.
22 B. Verhoff, S. S. Harilal, J. R. Freeman, P. K. Diwakar and A. Hassanein, *J. Appl. Phys.*, 2012, **112**, 093303.
23 S. S. Harilal, E. J. Kautz and M. C. Phillips, *Phys. Rev. E*, 2021, **103**, 013213.
24 R. R. D. Weeks, Y. Zhang, S. S. Harilal, M. C. Phillips and R. J. Jones, *J. Appl. Phys.*, 2022, **131**, 223103.
25 M. R. Savina, R. Trappitsch and B. H. Isselhardt, *Spectrochim. Acta, Part B*, 2018, **149**, 214.
26 N. Farid, S. S. Harilal, H. Ding and A. Hassanein, *J. Appl. Phys.*, 2014, **115**, 033107.
27 J. R. Freeman, S. S. Harilal, P. K. Diwakar, B. Verhoff and A. Hassanein, *Spectrochim. Acta, Part B*, 2013, **87**, 43.
28 S. S. Harilal, N. L. LaHaye and M. C. Phillips, *Opt. Express*, 2017, **25**, 2312.
29 M. C. Phillips, B. E. Brumfield, N. LaHaye, S. S. Harilal, K. C. Hartig and I. Jovanovic, *Sci. Rep.*, 2017, **7**, 3784.
30 G. Hull, E. D. McNaghten, C. A. Sharrad and P. A. Martin, *Spectrochim. Acta, Part B*, 2022, **190**, 106378.
31 P. J. Skrodzki, N. P. Shah, N. Taylor, K. C. Hartig, N. L. LaHaye, B. E. Brumfield, I. Jovanovic, M. C. Phillips and S. S. Harilal, *Spectrochim. Acta, Part B*, 2016, **125**, 112.
32 N. L. LaHaye, S. S. Harilal and M. C. Phillips, *Spectrochim. Acta, Part B*, 2021, **179**, 106096.
33 M. Miyabe, M. Oba, H. Iimura, K. Akaoka, A. Khumaeni, M. Kato and I. Wakaida, *Spectrochim. Acta, Part B*, 2015, **110**, 101.
34 M. Miyabe, M. Oba, K. Jung, H. Iimura, K. Akaoka, M. Kato, H. Otobe, A. Khumaeni and I. Wakaida, *Spectrochim. Acta, Part B*, 2017, **134**, 42.
35 A. Kuwahara, Y. Aiba, T. Nankawa and M. Matsui, *J. Anal. At. Spectrom.*, 2018, **33**, 893.
36 A. Kuwahara, Y. Aiba, S. Yamasaki, T. Nankawa and M. Matsui, *J. Anal. At. Spectrom.*, 2018, **33**, 1150.
37 A. Kuwahara, Y. Aiba, T. Nankawa and M. Matsui, *J. Anal. At. Spectrom.*, 2021, **42**, 134.
38 A. Kuwahara, Y. Aiba and M. Matsui, *ACS Omega*, 2021, **6**, 11750.

39 C. Vitelaru, L. de Poucques, T. M. Minea and G. Popa, *J. Appl. Phys.*, 2011, **109**, 053307.
40 H. Scheibner, St. Franke, S. Solyman, J. F. Behnke, C. Wilke and A. Dinklage, *Rev. Sci. Instrum.*, 2002, **73**, 378.
41 R. B. Wright, M. J. Pellin, D. M. Gruen and C. E. Young, *Nucl. Instrum. Methods*, 1980, **170**, 295–302.
42 Atomic spectral line database from CD-ROM 23 of R. L. Kurucz, available at **https://lweb.cfa.harvard.edu/amp/ampdata/kurucz23/sekur.html**.
43 M. Miyabe, M. Oba, H. Iimura, K. Akaoka, Y. Maruyama, H. Ohba, M. Tampo and I. Wakaida, *Appl. Phys. A*, 2013, **112**, 87.
44 M. Miyabe, M. Oba, H. Iimura, K. Akaoka, Y. Maruyama, H. Ohba, M. Tampo and I. Wakaida, *J. Appl. Phys.*, 2012, **112**, 123303.
45 B. A. Bushaw and M. L. Alexander, *Appl. Surf. Sci.*, 1998, **127**, 935.
46 N. M. Bulgakova, A. V. Bulgakov and O. F. Bobrenok, *Phys. Rev. E*, 2000, **62**, 5624.
47 M. Skočić, D. Dojić and S. Bukvić, *J. Quant. Spectrosc. Radiat. Transfer*, 2019, **227**, 57.
48 S. S. Harilal, C. V. Bindhu, M. S. Tillack, F. Najmabadi and A. C. Gaeris, *J. Phys. D:Appl. Phys.*, 2002, **35**, 2935.
49 C. Focsa, S. Gurlui, P. Nica, M. Agop and M. Ziskind, *Appl. Surf. Sci.*, 2017, **424**, 299.
50 K. Yahiaoui and S. M. Aberkane, *Spectrochim. Acta, Part B*, 2021, **180**, 106197.
51 E. H. Kwapis, M. Hewitt and K. C. Hartig, *Opt. Express*, 2023, **31**, 10694.
52 K. Yahiaoui, S. Abdelli-Messaci, S. M. Aberkane, T. Kerdja and H. Kellou, *Spectrochim. Acta, Part B*, 2014, **93**, 20.
53 K. Yahiaoui, S. Abdelli-Messaci, S. M. Aberkane, M. Siad and A. Kellou, *Appl. Phys. A*, 2017, **123**, 464.
54 S. S. Harilal, C. V. Bindhu, M. S. Tillack, F. Najmabadi and A. C. Gaeris, *J. Appl. Phys.*, 2003, **93**, 2380.
55 A. K. Sharma and R. K. Thareja, *Appl. Phys. Lett.*, 2004, **84**, 4490.
56 D. B. Geohegan, *Thin Solid Films*, 1992, **220**, 138.
57 B. Y. Man, X. T. Wang and A. H. Liu, *J. Appl. Phys.*, 1998, **83**, 3509.
58 M. S. Finko and D. Curreli, *Phys. Plasmas*, 2018, **25**, 083112.
59 M. S. Finko, D. Curreli, D. G. Weisz, J. C. Crowhurst, T. P. Rose, B. Koroglu, H. B. Radousky and M. R. Armstrong, *J. Phys. D: Appl. Phys.*, 2017, **50**, 485201.
60 E. J. Kautz, M. C. Phillips and S. S. Harilal, *Anal. Chem.*, 2020, **92**, 13839.
61 E. J. Kautz, P. J. Skrodzki, M. Burger, B. E. Bernacki, I. Jovanovic, M. C. Phillips and S. S. Harilal, *J. Anal. At. Spectrom.*, 2019, **34**, 2236.
62 S. S. Harilal, B. E. Brumfield, B. D. Cannon and M. C. Phillips, *Anal. Chem.*, 2016, **88**, 2296.
63 P. J. Skrodzki, M. Burger, I. Jovanovic, M. C. Phillips, J. Yeak, B. E. Brumfield and S. S. Harilal, *Phys. Plasmas*, 2019, **26**, 083508.
64 E. H. Kwapis, J. W. Posey, E. Medici, K. Berg, R. W. Houim and K. C. Hartig, *Phys. Chem. Chem. Phys.*, 2023, **25**, 15666.
65 S. S. Harilal, E. J. Kautz, B. E. Bernacki, M. C. Phillips, P. J. Skrodzki, M. Burger and I. Jovanovic, *Phys. Chem. Chem. Phys.*, 2019, **21**, 16161.
66 M. C. Phillips, E. J. Kautz and S. S. Harilal, *Opt. Lett.*, 2023, **48**, 1942.
67 M. P. Polek, M. C. Phillips, F. N. Beg and S. S. Harilal, *AIP Adv.*, 2024, **14**, 025043.
68 Z. Zhang and G. Gogos, *Phys. Rev. B:Condens. Matter Mater. Phys.*, 2004, **69**, 235403.